Study of the temperature and pressure dependent structural properties of alkali hydrido-*closo*-borates compounds

Romain Moury[ab]*, Zbigniew Łodziana[c]*, Arndt Remhof[d], Léo Duchêne[da], Elsa Roedern[d], Angelina Gigante[ad] and Hans Hagemann[a]*

[a] Department of Physical Chemistry, University of Geneva, 30 Quai E. Ansermet, Geneva, 1211, Switzerland
[b] Institut des Molécules et Matériaux du Mans, University of le Mans, Avenue Olivier Messiaen, Le Mans, 72085, France
c Institute of Nuclear Physics, Polish Academy of Sciences, ul. Radzikowskiego 152, Kraków, 31342, Poland
[d] Empa, Swiss Federal Laboratories for Materials Science and Technology, Überlandstrasse 129, Dübendorf, 8600, Switzerland

*corresponding author: romain.moury@univ-lemans.fr, Zbigniew.Lodziana@ifj.edu.pl

Abstract.

In this work we report on the structural properties of alkali hydrido-*closo*-(car)borates, a promising class of solid-state electrolyte materials, using high-pressure and temperature dependent X-ray diffraction experiments combined with DFT calculations. The mechanical properties are determined from pressure dependent diffraction studies and DFT calculations; the shear moduli appear to be very low for all studied compounds revealing their high malleability (that can be beneficial for the manufacturing and stable cycling of all-solid-state batteries). The thermo-diffraction experiments also reveal a high coefficient of thermal expansion for these materials. We discover a pressure induced phase transition for $K_2B_{12}H_{12}$ from *Fm*-3 to *Pnnm* symmetry around 2GPa. A temperature induced phase transition for $Li_2B_{10}H_{10}$ was also observed for the first time by thermodiffraction and the crystal structure solved combining experimental data and DFT calculations. Interestingly, all phases of the studied compounds (including newly discovered high pressure and high temperature phases) may related via group-subgroup relationship, with the notable exception of the room temperature phase of $Li_2B_{10}H_{10}$.

Introduction.

Since the discovery of superionic conductivity in the high temperature phase of $Na_2B_{12}H_{12}$,[1] there has been an increasing interest in hydrido – *closo* – (car)borates, and hydrido – *nido* – (car)borates and their solid solutions,[2–11] as well as their halogenated derivatives.[12] Several of these compounds or solid solutions exhibit very high ionic conductivities above 1 mS/cm at room temperature and they are chemically and electrochemically very stable.[13,14] Recently, some prototype of all-solid-state batteries using hydrido – *closo* – (car)borates as electrolytes have demonstrated very promising

performances.[15,16] Furthermore novel cost effective methods have been developed to synthesis hydrido – *closo* – borates from solution, [17,18] allowing electrodes impregnations to notably improve ionic contact between the electrode and electrolyte.[19] These results demonstrate that this family presents many excellent properties as solid ionic conductors for new generations of all-solid-state batteries.

Understanding the bulk mechanical properties of solid electrolyte in general and H-*c*-B in particular is crucial to develop manufacturing method for all-solid-state batteries as well as to improve their cycling stability.[20] For example, charging and discharging cycles can induce volume changes of the electrodes materials, which should be accommodated by the solid electrolyte without mechanically disrupting the electrode-electrolyte interface. Some of the authors have demonstrated that a solid electrolyte based on a solid solution between H-*c*-B and hydrido-*closo*-carborate is stable for at least 800 charging/discharging cycles.[21] Mechanical properties such as the shear modulus of solid electrolyte is also considered as an important parameter in some models of dendrite formation in solid electrolytes.[22] Thermal expansion of the materials constituting the battery may as well induce mechanical stresses when the battery is subject to overheating. A colossal barocaloric effect has also been predicted for $Li_2B_{12}H_{12}$,[23] hence the behavior of this family of materials upon pressure and temperature are important aspects in understanding these properties. Furthermore, while the fundamental of the crystal chemistry of hydrido – *closo* – borates is well established,[24] some pieces are still missing. For instance, a temperature induced phase transition has been observed by DSC experiment for $Li_2B_{10}H_{10}$ and $(K,Cs)_2B_{12}H_{12}$ though no crystal structure was given.[25,26] In addition, only few reports on high pressure behavior for this family of compounds exist except for $(Na,Cs)_2B_{12}H_{12}$.[27,28] In this context, insight in their structural behavior under external stimuli (pressure, temperature) is a critical aspect to extract some fundamental knowledge and physical properties, as the Coefficients of the Thermal Expansion (CTE) and the isothermal compressibility, of this class of compounds. In this work, we have investigated the temperature and pressure dependent X-ray diffraction of a series of Hydrido-*closo*-Borates (H-*c*-B) and of $NaCB_{11}H_{12}$ to provide experimental data of the thermal expansion and compressibility of constituents of solid state ionic conductors for sodium and lithium. In our investigations, we have discovered and solved two new polymorphs, namely the high temperature (ht, for temperature above room temperature) β-$Li_2B_{10}H_{10}$, and the high-pressure (hp) β-$K_2B_{10}H_{10}$. These experimental results are completed by theoretical DFT calculations. And a comprehensive analysis of the structural and vibrationnal behavior of these materials is given.

Background

Even though H-*c*-B exhibit a very rich crystal chemistry with numerous temperature and pressure induced phase transition, they share most of the time common aristotypes such as: cubic close packing (*ccp*), hexagonal close packing (*hcp*) and body center cubic (*bcc*) arrangement.[24] Along the series of alkali dodeca H-*c*-B, at ambient pressure and temperature, the larger cations $(K,Rb,Cs)_2B_{12}H_{12}$ crystallize in the cubic *Fm*-3 space group and $Li_2B_{12}H_{12}$ in the cubic *Pa*-3 space group with

undistorted *ccp* while $Na_2B_{12}H_{12}$ adopts the monoclinic $P2_1/c$ symmetry with the distorted *ccp*. With respect to the deca H-*c*-B, $(Na,K,Rb)_2B_{10}H_{10}$ adopt the monoclinic $P2_1/c$ space group with distorted *ccp*, *hcp* and *hcp* respectively whereas $Li_2B_{10}H_{10}$ stand as an exception with the hexagonal space group $P6_422$ without cubic or hexagonal compact underlying packing. Their temperature induced polymorphic phase transition have been studied and solved for, $(Li,Na,Rb,Cs)_2B_{12}H_{12}$ and for $Na_2B_{10}H_{10}$,[26,29,30] while pressure induced phase transitions have been investigated solely for $Na_2B_{12}H_{12}$. It is undergoing two phase transitions at relatively low pressure: $P2_1/c$ → [0.3-0.8 GPa] *Pbca* → [5.7-8.1 GPa] *Pnnm*.[27] **Fig. 1** gathers the different symmetries encountered for all the known H-*c*-B together with their underlying packing in a group-subgroup graph. It is worth noting that most of the H-*c*-B exhibit a direct group-subgroup relationship (red path on **Fig. 1**) that can come into play for the phase transitions for these compounds as discussed in detail for the pressure-induced transitions of $Na_2B_{12}H_{12}$.[27] Furthermore, the preferred packing for this family is *ccp* with exception for ht polymorphs of $Na_2B_{12}H_{12}$ adopting the *bcc* packing for the ht1-β-$Na_2B_{12}H_{12}$ and ht2-γ-$Na_2B_{12}H_{12}$. $Na_2B_{12}H_{12}$ possesses the richest phase diagram among all the H-*c*-B and it is the only one found in the *bcc* arrangement which is known to favor ionic conductivity.[31]

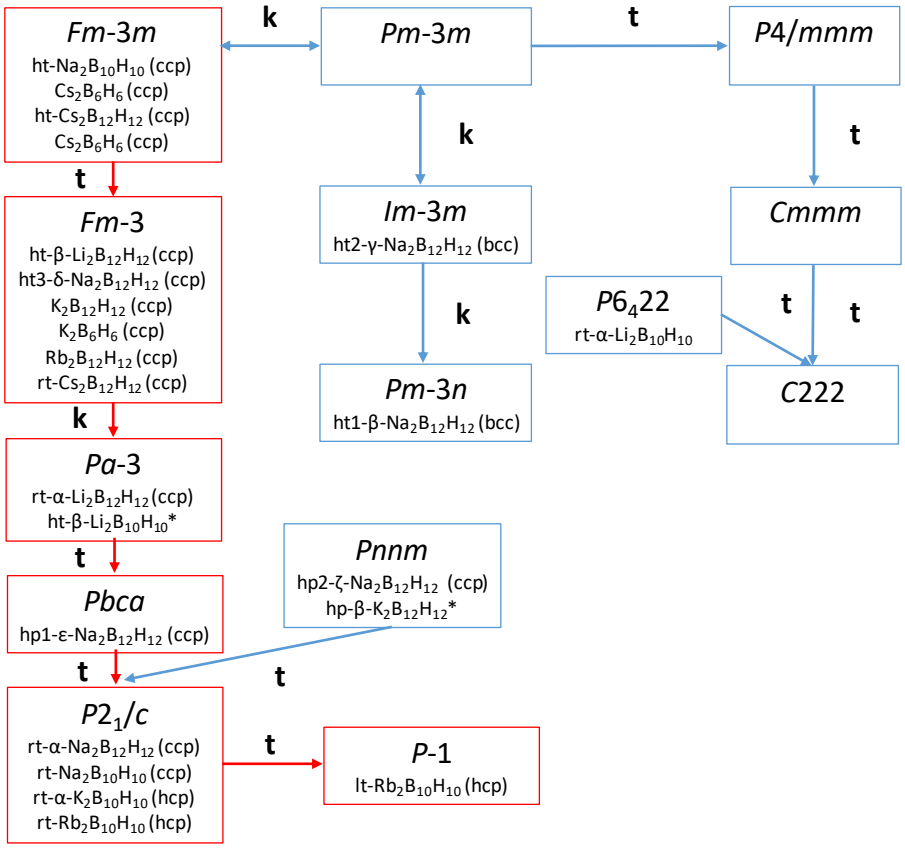

Figure 1. Group-subgroup relationship between the hydrido-*closo*-borates. **t** stands for *translationengleich* and **k** *klassengleich* subgroups. The asterisk * indicates the crystal structures determined in this work. rt and lt stand for room temperature and low temperature, here bellow 250 K, respectively.

Result and discussion.

Pressure dependence

High pressure X-ray diffraction

Six different samples $(Li,Na,K)_2B_{12}H_{12}$, $(Li,K)_2B_{10}H_{10}$ and $NaCB_{11}H_{12}$ were investigated at Swiss Norwegian Beam Line (SNBL) in order to study their behavior under pressure. Except for $Na_2B_{12}H_{12}$, for which the hp phase transitions were already described,[27] $K_2B_{12}H_{12}$ also undergoes to a reversible phase transition at pressure above 2 GPa toward a polymorph isostructural to hp2-ζ-$Na_2B_{12}H_{12}$ with the orthorhombic *Pnnm* symmetry (**Fig. 2 a**). The cell parameters were first determined using Pawley refinement with hp2-ζ-$Na_2B_{12}H_{12}$ as first input and manually increased to fit the diffraction pattern, once good approximation was found the refinement was carried out. The Rietveld refinement was subsequently achieved with the as-obtained cell parameters and hp2-ζ-$Na_2B_{12}H_{12}$ atomic positions that enabled obtaining hp-β-$K_2B_{12}H_{12}$ with a = 7.1670(13) Å, b = 9.212(6) Å and c = 7.560 (3) Å (**Fig. 2 b**). Despite the low quality of the pattern, due to the strains and preferential orientations induced by the pressure, refinement successfully converged with the reliability factors of *Rwp* = 1.88, *Rp* = 1.16 and GoF = 6.5 (**Fig. S1**).

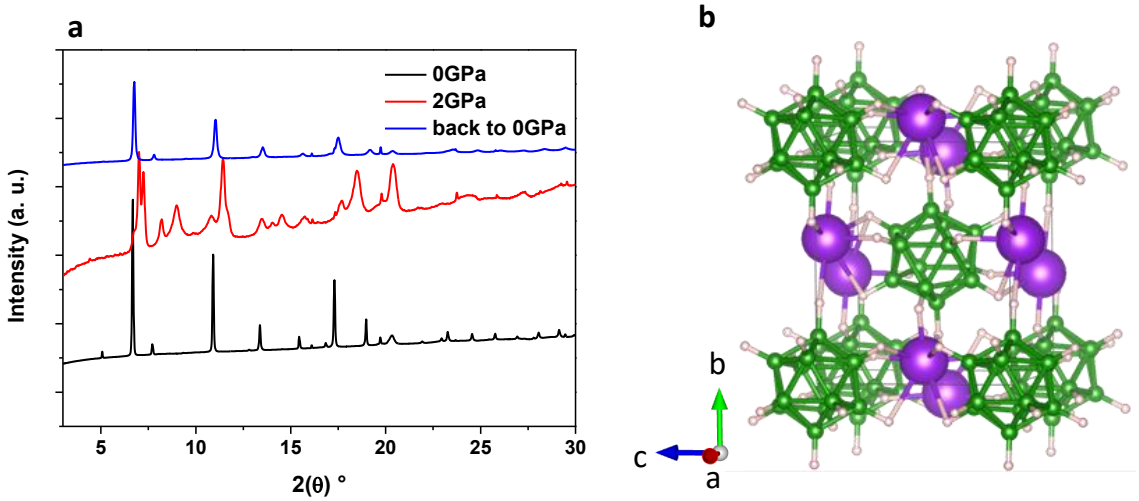

Figure 2. Diffraction patterns of $K_2B_{12}H_{12}$ at 0 GPa (black), 2 GPa (red) and back to ambient pressure (blue) depicting it reversible pressure induced phase transition (a). Representation of the hp-β-$K_2B_{12}H_{12}$ crystal structure (b).

Owing to the low quality of the diffraction pattern, DFT calculations were performed to further confirm the stability of the *Pnnm* symmetry. The diffraction peak at 8.2° cannot be explain by the refinement, which can be due either to the remaining 111 reflection from the lp-phase of another polymorph. The calculated pressure dependence of the free energy ($F = E_0 + pV$) reveal the phase transition of $K_2B_{12}H_{12}$ (*Fm*-3 → *Pnnm*) at the pressure 3.58 GPa hence further confirm the experimental data (**Fig. S2**). The phase transition is accompanied by ~7% specific volume change indicating first order transition. While a group-subgroup relationship exists between *Fm*-3 and *Pnnm* a

direct comparison of both structures does not allow identifying the transition mechanism. A transformation of the hp-β-$K_2B_{12}H_{12}$ *Pnnm* phase into $P2_1/c$, with $P2_1/c \subset Fm\text{-}3$, using the following matrix: $\mathbf{a}_{mono} = -\mathbf{b}_{ortho} - \mathbf{c}_{ortho}$, $\mathbf{b}_{mono} = \mathbf{a}_{ortho}$ and $\mathbf{b}_{mono} = -\mathbf{b}_{ortho} + \mathbf{c}_{ortho}$ with an origin shift $\mathbf{c}_{mono} = \mathbf{c}_{ortho} + 1/2$ (**Fig. S3**) was performed prior to the comparison. The phase transition is diplacive combining a diffusionless (martensitic-like) transformation for the $B_{12}H_{12}^{2-}$ units with the displacement of potassium cation similarly to $Na_2B_{12}H_{12}$.[27] The martensitic-like transition is displayed in **Fig. S4** during which the cubic lattice is transformed into the monoclinic one. The deformation leads to the following high values of the Lagrangian strain tensor with $e_{11} = e_{33} = 0.1515$, $e_{22} = -0.2643$ and $e_{31} = e_{13} = 0.1272$ hence must be taken into account to treat the phase transition using a finite strain approach. As consequence, the Landau free energy must be built with an order parameter-strain coupling.[32] Using group-theory analysis with amplimode,[33,34] in Bilbao Crystallographic Server, one can identify that the symmetry reduction from *Fm*-3 to $P2_1/c$ is driven by three one dimensional irreducible representations (irreps) Γ^{4+} at wave vector *k* (0,0,0), X^{1+} and X^{+2} and one three dimensional X^{2+} irrep at *k* (0,1,0).

Mechanical properties.

In the pressure range [0-6 GPa], $Li_2B_{12}H_{12}$, $(Li,K)_2B_{10}H_{10}$ and $NaCB_{11}H_{12}$ do not undergo pressure-induced phase transition. Together with hp2-ε-$Na_2B_{12}H_{12}$ and hp-β-$K_2B_{12}H_{12}$ their cell volumes were determined as a function of the pressure. When the data allowed, experimental bulk moduli were determined by fitting the Murnaghan equation of state (**Eq. 1**) with the experimental data (**Fig. S5**) and results are gathered in **Table 1**.

$$V(P) = V_0\left(1 + K_0{}'\frac{P}{K_0}\right)^{-1/B_0{}'} \quad (1)$$

The experimental bulk moduli determined for the abovementioned compounds are in the range 16.3 to 25.5 GPa revealing very high compressibility in good agreement with our previous study about $Na_2B_{12}H_{12}$.[27]

Elastic properties of the ordered phases of alkali H-*c*-B were also determined by DFT calculation (**Table 1).** They are in good agreement with experimental values validating our calculation strategy. One has to keep in mind that calculated values correspond to the adiabatic constants, while experimental data are for isothermal values. Evolution of the bulk (K) and the shear (G) moduli as a function of the volume per formula unit is represented in **Fig. 3**. For Li cation the bulk and the shear moduli are systematically larger than for other elements of the group. Along the series $M_2B_{10}H_{10}$, the bulk modulus somewhat decreases for heavier cation while for the $M_2B_{12}H_{12}$ family one can observe a slight increase with the mass of the cation. The shear modulus does not follow any obvious trend, however it is significantly smaller than for oxides or sulfides (>10 GPa)[35]. This is an indication of

malleability of these compounds, especially with dodeca H-*c*-B anions, for example following Pugh criterion for ductile materials is having ratio K/G > 1.75.[36]

Table 1. Summary of the bulk (K) and shear (G) moduli obtained experimentally and by DFT of the alkali deca and dodeca H-*c*-B. The indexes r and v stands for Reuss and Voigt limit.

Compound	Space group	G_r [GPa]	G_v [GPa]	K_r [GPa]	K_v [GPa]	K_{exp}
$Li_2B_{10}H_{10}$	*P*6$_4$22 (#181)	6.20	7.43	20.01	20.46	16.3(4.6)
$Li_2B_{12}H_{12}$	*Pa* -3 (#205)	11.31	8.96	20.84	20.84	21.3(1.4)
$Na_2B_{10}H_{10}$	*P*2$_1$/*c* (#14)	8.35	7.21	19.08	19.24	-
$Na_2B_{12}H_{12}$	*P*2$_1$/*c* (#14)	2.11	6.08	7.20	16.10	13.1(6)
$K_2B_{10}H_{10}$	*P*2$_1$/*c* (#14)	8.38	7.24	19.07	19.21	25.5(2.5)
$K_2B_{12}H_{12}$	*Fm*-3 (#202)	7.41	5.99	16.85	16.49	-
$Rb_2B_{10}H_{10}$	*P*2$_1$/*c* (#14)	5.25	4.45	17.10	17.56	-
$Rb_2B_{12}H_{12}$	*Fm*-3 (#202)	7.34	5.94	16.80	16.80	-
$Cs_2B_{10}H_{10}$	*P*2$_1$/*c* (#14)	2.33	3.14	10.25	15.27	-
$Cs_2B_{12}H_{12}$	*Fm*-3 (#202)	6.17	4.91	14.68	14.68	-

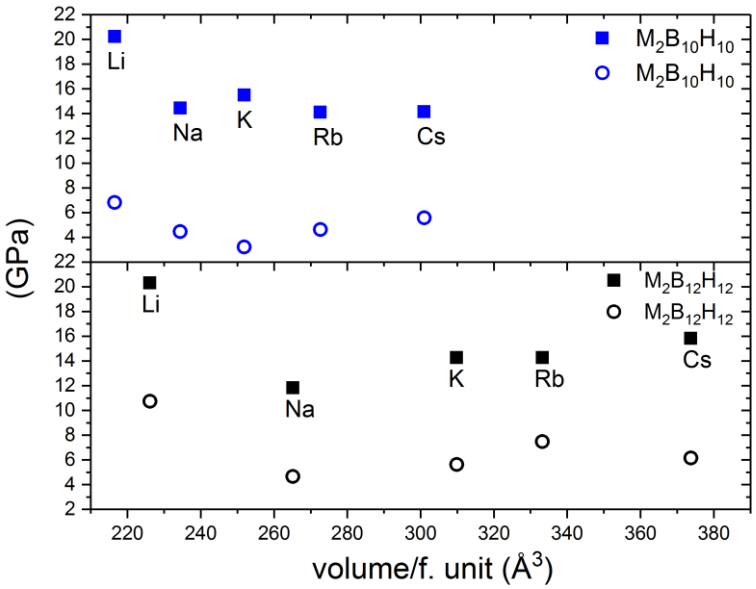

Figure 3. Calculated bulk (squares) and shear (circles) moduli for alkali metal deca- and dodeca- H-*c*-B. The average $(X_r+X_v)/2$ values are presented.

The relatively large compressibility and malleability of H-*c*-B is beneficial for solid-state battery manufacturing making it easier to densify the solid-electrolyte layer and to achieve intimate contact with the electrode. If a good contact between H-*c*-B and active material is established (via solution processing for example)[19] it can be maintained upon cycling thanks to their high deformability. It is

worth mentioning that mechanical properties obtained from structural studies cannot always be translated to bulk properties in a battery where a solid electrolyte is typically a pressed polycrystalline powder. Nevertheless, H-c-B have proven to maintain stable interfaces in all-solid-state-batteries upon many cycles, including without applying significant external mechanical pressure.[21] The experimental and theoretical values appear to be characteristic for the entire series of compounds and can thus be extrapolated to predict the behavior of new ionic conductors based on H-*c*-B and derived compounds. Additionally, the very low shear moduli is an indication that such materials easily adapt to the structural changes of the electrode.

Temperature dependence

High temperature X-ray diffraction

Most of the crystal structures of deca and dodeca H-*c*-B of alkali metals are known for the low and high temperature polymorphs,[24,26,30] with exceptions concerning the high temperature phases of $Li_2B_{10}H_{10}$ and $(K,Rb)_2B_{12}H_{12}$ which were observed by DSC measurements but the structure has never been solved.[25,26] $K_2B_{12}H_{12}$ undergoes to a phase transition at about 540°C which is around the transformation temperature of the glass capillary hence the transition was not recorded during our experiment. Nonetheless we did observe a phase transition for rt-α-$Li_2B_{10}H_{10}$ starting to transform into ht-β-$Li_2B_{10}H_{10}$ at 361°C. From this temperature both polymorphs coexist up to 384°C temperature at which rt-α-$LiB_{10}H_{10}$ totally transforms into ht-β-$LiB_{10}H_{10}$. At 390°C the diffraction peaks ht-β-$LiB_{10}H_{10}$ start to decrease with the appearance of an amorphous and a new, crystal phase. The possible nature of this new crystal structure will be discussed below. From 430°C only the new and amorphous phases are present up to 453°C, the temperature at which the compound becomes amorphous. **Fig. 4** displays the diffraction patterns for the different steps described. These observations are in good agreement with the previous study on $Li_2B_{10}H_{10}$ thermal behavior in which an entropically driven order-disorder phase transition was suggested.[25] However, the appearance of the unidentified crystal phase was never reported; due to the low quality of the diffraction pattern a direct structural determination was not possible during our experiments but the structure was likely determined with support of DFT calculations (see below).

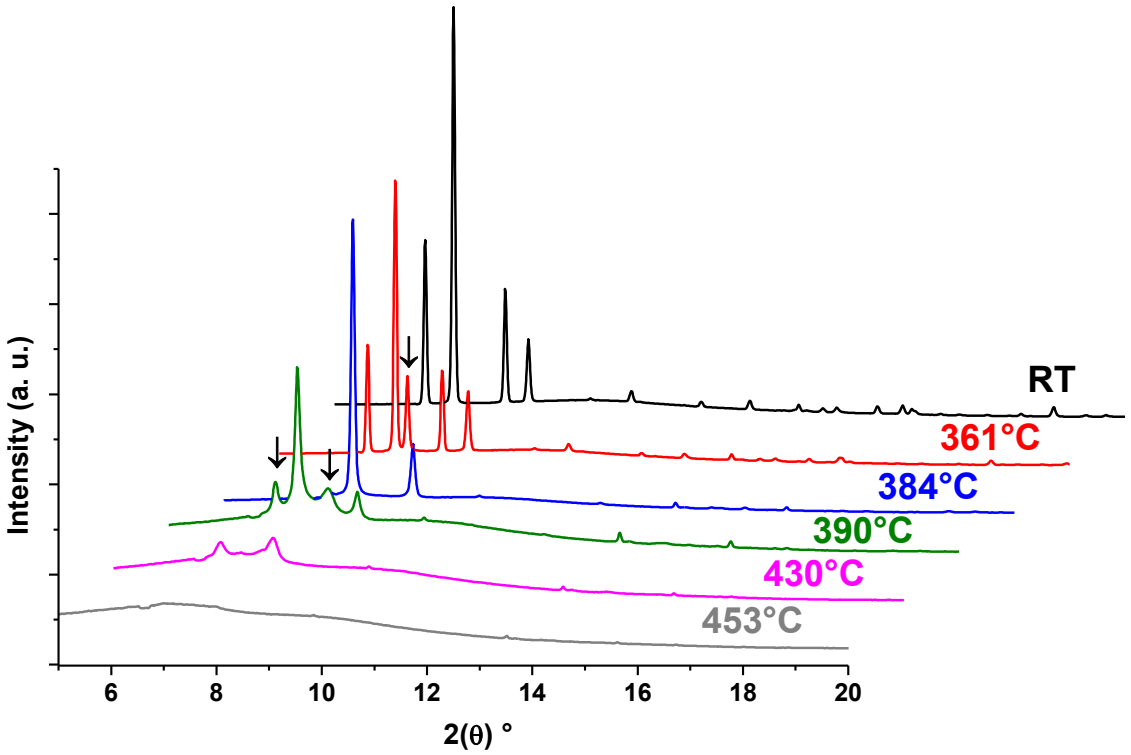

Figure 4. Temperature dependency of the diffraction patterns for $Li_2B_{10}H_{10}$. At RT only rt-α-$LiB_{10}H_{10}$ is present, at 361°C appearance of ht-β-$LiB_{10}H_{10}$ (arrow) and coexistence of both polymorphs up to 384°C, at 390°C appearance of the unidentified phase (arrow) and coexistence of both phases up to 430°C and at 453°C amorphization of the material.

With regards to ht-β-$Li_2B_{10}H_{10}$ the phase appears to be isostructural to $Li_2B_{12}H_{12}$ and its pattern can be indexed with a cubic lattice with a = 9.5316(3) Å and V = 865.96(7) $Å^3$. The structure can be refined in two different space groups namely *Fm*-3*m* and *Pa*-3 with similar agreement factors (*Rwp* = 4.2 and 4.0 for *Pa*-3 and *Fm*-3*m* respectively). In both structures, the $B_{10}H_{10}^{2-}$ ions are orientationally disordered as suggested in the previous study.[25]

DFT calculations for ht-β-$Li_2B_{10}H_{10}$

These structures differ in the average orientation of $B_{10}H_{10}^{2-}$anions, as shown in the **Fig. S6**. For the structure with *Pa*-3 symmetry the $B_{10}H_{10}^{2-}$ anions are oriented such that the longer anion axis is along one of the principal lattice directions (3 preferred orientations). This results an average quasi-octahedral shape. For *Fm*-3*m* symmetry there are four orientations along the cubic unit cell diagonals preferred by $B_{10}H_{10}^{2-}$ anions. They average to the effective cubic shape of anion, see **Fig. S6**. Since both geometrical figures, the cube and the octahedron have the same number of symmetry elements the distinction between two crystal structures of $Li_2B_{10}H_{10}$ must be related to the positions of cations which is coupled to the anion orientation. In order to determine which of the two orientations are the preferred (has larger cohesive energy) we performed series of DFT calculations. Since the high temperature phase is disordered, calculations procedure was developed. The structures with random

anion orientations/cation distribution were used to calculate energy; details are presented in the Supporting Information. The energy distribution for the atomic configurations in the cubic phase of $Li_2B_{10}H_{10}$ is presented in **Fig. 5**. It consists of separated energy maxima starting with $\Delta E = 0.014$ eV/atom above the $P6_422$ ground state energy up to $\Delta E = 0.035$ eV/atom for the least stable configurations. For four selected regions the radial distribution function (rdf) for Li – H separation were calculated, as shown in the inserts in **Fig. 5**. In general rdf for the most stable configurations resembles this of the low temperature phase, where two Li – H distances at 2.1 Å and 2.3 Å are present (they are larger than 2.028 Å, 2.044 Å and 2.216 Å reported for experimental structure of $Li_2B_{10}D_{10}$)[25]. For the configurations that are the least stable the Li – H separation strongly differs from the low temperature one: Li – H spacing has broad distribution within the range from 1.9 Å to 2.7 Å. Such short interatomic distances indicate that Li is closely connected to anions. This can be seen in **Fig. 5** where distribution of cations is shown for the structure with lowest energy, and cations confined to the tetrahedral interstitial voids. The least stable configuration cations are located at tetrahedral facets rather than in tetrahedral center. The projection of $B_{10}H_{10}^{2-}$ anion orientations on (*a*,*b*) crystal plane indicate they are oriented with longer axis along (100), (010) or (001) lattice directions except for the least stable structure where the orientation is along unit cell diagonals, see **Fig. 5**. This point toward *Pa*-3 space group symmetry for the high temperature phase of $Li_2B_{10}H_{10}$ and possible second phase transition to *Fm*-3*m* space group at higher temperatures prior the thermal decomposition of compound. Having this in mind one can suggest that the unidentified ht phase could be the cubic *Fm*-3*m*. A Rietveld refinement was then performed with a = 10.219(3) Å, however owing to the poor quality of the diffraction pattern the fit was not optimal but the solution cannot be excluded. Additional work would be necessary to demonstrate this last transition.

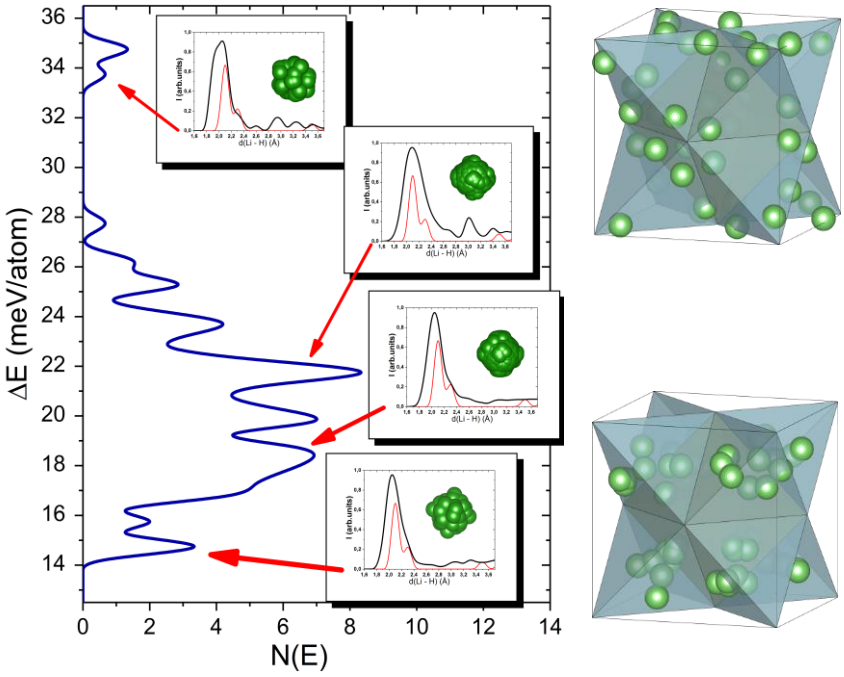

Figure 5. The energy distribution of $Li_2H_{10}H_{10}$ in the cubic *ccp* structure with respect to the *hcp* ($P6_422$) ground state. The inserts show radial distribution function for Li – H separation, red line is for the reference hexagonal structure. The green spheres are projections of anions on (a,b) plane for given energy range. The right side shows distribution of cations corresponding to the configurations with the lowest and highest energy, for simplicity only coordination tetrahedra of the fcc lattice are shown with light blue shade.

Coefficient of the Thermal Expansion

Coefficients of the Thermal Expansion (CTE) were determined for several alkali hydrido-*closo*-(car)borates studied here by fitting the evolution of the volume as a function of the temperature to a polynomial function (**Eq. 2**). The CTE α can be determined using **Eq. 3**. The results are gathered in **Table 2.**

$$V\left(\mathring{A}^3\right) = V_0 + A \cdot T + B \cdot T^2 + C \cdot T^3 \quad (2)$$

$$\alpha(K^{-1}) = \frac{1}{V}\left(\frac{\partial V}{\partial T}\right)_p = \alpha_0 + D \cdot T + E \cdot T^2 \quad (3)$$

The relatively high value of the CTE, compared to oxides which are usually two orders of magnitude lower than this family of compounds, point out a strong dilatation for these materials with temperature. This feature could induce mechanical stresses between the different component of the battery cathode (usually oxide-based), anode and electrolyte. These mechanical stressed would be detrimental in case of overheating. However the very low shear moduli for these compounds could overcome this issue, the material will flow and with proper construction hence shall not affect the interface. Low shear moduli can be seen as the behavior of the materials, upon external stimuli, approaching the one of the liquid. Additionally elastic constants (Table 1.) indicate malleability of this class of materials. The thermal expansion is a manifestation of the anharmonicity of the lattice vibrations and fitting the evolution of the volume as a function of the temperature with polynomial of order ≥ 2 indicate a strong anharmonicity, related to the orientational disorder of anions.

Table 2. Summary of the coefficients (V_0, A, B, C) of the polynomials used to fit the evolution of the volume of the cells as a function of the temperature together with the coefficients (α_0,D,E) of the equations of the CTE as a function of the temperature and the average of the CTE (α(avg)) calculated on the indicated temperature range.

Compound	**Space group**	**V_0 (Å^3)**	**A**	**B**	**C**	**α (avg) (K^{-1})**	**α_0 (K^{-1})**	**D (K^{-2})**	**E (K^{-3})**	**T (K)**
$Li_2B_{10}H_{10}$	*P*6$_4$22	600.9(3)	0.020(1)	3.9(1) 10^{-5}	-	0.95 10^{-4}	3.333(3) 10^{-5}	1.342(1) 10^{-7}	-1.67(1) 10^{-11}	320-620
$Na_2B_{10}H_{10}$	*P*2$_1$/*c*	870.8(3)	0.123(1)	-	-	1.35 10^{-4}	1.410(1) 10^{-4}	-	-	300-380
$Na_2B_{10}H_{10}$	*Fm*-3*m*	891.2(4)	0.1376(7)	-	-	1.4 10^{-4}	1.533(7) 10^{-4}	-	-	400-795
$Na_4(B_{10}H_{10})(B_{12}H_{12})$	*Fm*-3*m*	900.5(6)	0.468(3)	-5.50(7) 10^{-4}	3.19(4) 10^{-7}	1.8 10^{-4}	4.69(1) 10^{-4}	-1.098(3) 10^{-6}	9.32(2) 10^{-10}	300-796
$K_2B_{12}H_{12}$	*Fm*-3	1141(1)	0.1838(2)	-	-	1.4 10^{-4}	1.90(3) 10^{-5}	-	-	305-724
$NaCB_9H_{10}$	*Pna*2$_1$	406.1(2)	0.1129(4)	-	-	2.5 10^{-4}	2.751(1) 10^{-4}	-	-	325-500
$Na_2B_{12}H_{12}$	*P*2$_1$/*c*	492	0.19	-3.8 10^{-4}	3.67 10^{-7}	1.3 10^{-4}	3.902 10^{-4}	7.723 10^{-7}	7.459 10^{-10}	273-540
$Na_2B_{12}H_{12}$	*Pm*-3*n*	457.9	0.12	-	-	2.3 10^{-4}	2.621 10^{-4}	-	-	540-580
$Na_2B_{12}H_{12}$	*Im*-3*m*	471.4	0.24	-	-	1.8 10^{-4}	5.091 10^{-4}	-	-	580-700
$Na_2B_{12}H_{12}$	*Fm*-3*m*	1051.1	0.14	-1.88 10^{-5}	-	1.1 10^{-4}	1.109(1) 10^{-4}	-1.075(6) 10^{-11}	-	540-750

Structural and vibrational analysis

Symmetry analysis points out to relations between space group symmetry of all alkali metal deca- and dodeca H-*c*-B. The low temperature hexagonal phase of $Li_2B_{10}H_{10}$ is somehow an exception from the family of structures originating from *Pm*-3*m* group.

In order to better understand the similarities between this family of compounds, below we report on structural and vibrational analysis. In **Fig. 6** the distribution of the zone center modes for alkali metal deca and dodeca H-*c*-B together with the radial distribution function for metal-hydrogen separation is displayed. With regards to deca H-*c*-B a clear division into two groups is apparent: Li, Na show short separation between hydrogen and metal that can be correlated with broader extend of the lattice modes. Especially for lithium the lattice modes go beyond 250 cm^{-1} which is an indication of direct and strong Li – $B_{10}H_{10}^{2-}$ interaction. More detailed information on internal $B_{10}H_{10}^{2-}$ vibrations can be found elsewhere,[37,38] however the splitting of B-H modes (>2400 cm^{-1}) is related to the bond distortion and the internal *closo* – cage vibrations in the range 400 – 1200 cm^{-1} are modified by small deformations of anion. The largest splitting of the highest frequency modes (B-H stretching modes) is observed for the heaviest cations, K, Rb, and Cs. This is related to the *hcp* packing of anions,[24] rather than *ccp* that is observed for Li and Na, and symmetry of $B_{10}H_{10}^{2-}$ molecule. This anion has point group symmetry *D*4*d* as for capped square antiprism, see **Fig. 7**. Distribution of cations is compatible with C4 and S8 symmetry elements of the molecule thus the differences can be ascribed to packing of anions.

For these modes similarities for K, Rb, and Cs are visible, which would be expected as these compounds have the same symmetry for the same anions. A large splitting of B–H modes for K, Rb, and Cs deca H-*c*-B shall be noticed, they are related to the distribution of these cations in the lattice which will be discussed below. For compounds with Li and Na B–H stretching have distinct splitting of frequencies.[38] While the spectrum related to the internal vibrations of anions have similarities within each class of compounds the differences are related to different site symmetry of anion in Li and Na containing compounds. The largest differences between them are present in the upper range of lattice modes above 150 cm^{-1}. While for K, Rb, and Cs a clear gap between lattice and internal anion modes is present; this gap is smaller for Li and Na, especially for $Li_2B_{10}H_{10}$ there are lattice vibrations present above 250 cm^{-1}, for Na they are less extended as well as for icosahedral dodeca anion they extend to lower frequencies.

In **Fig. 6 c and d** the pair distribution function calculated for metal – hydrogen separation is presented. For both classes of compounds clear differences are visible between Li/Na and heavier metals. While well-defined Li – H separation just above 2 Å is visible for $Li_2B_{10}H_{10}$, these separations are still present in $Na_2B_{10}H_{10}$ with some additional peaks below 3 Å. All heavier alkali metals are separated from nearest hydrogen by more than 2.5 Å, and the distribution of M – H distances is not well defined

for deca H-*c*-B (**Fig. 6 c**), showing bond length distribution between 2.5 Å and 6 Å. The opposite is observed in dodeca H-*c*-B M–H spacing is well defined for Cs, Rb and K and it is decreasing with decreasing mass (radius) of metal cation (**Fig 6. d**). For Li and Na in dodeca H-*c*-B this spacing is smaller (~2 Å) and distance distribution similar to this in deca H-*c*-B is clear, also for sodium.

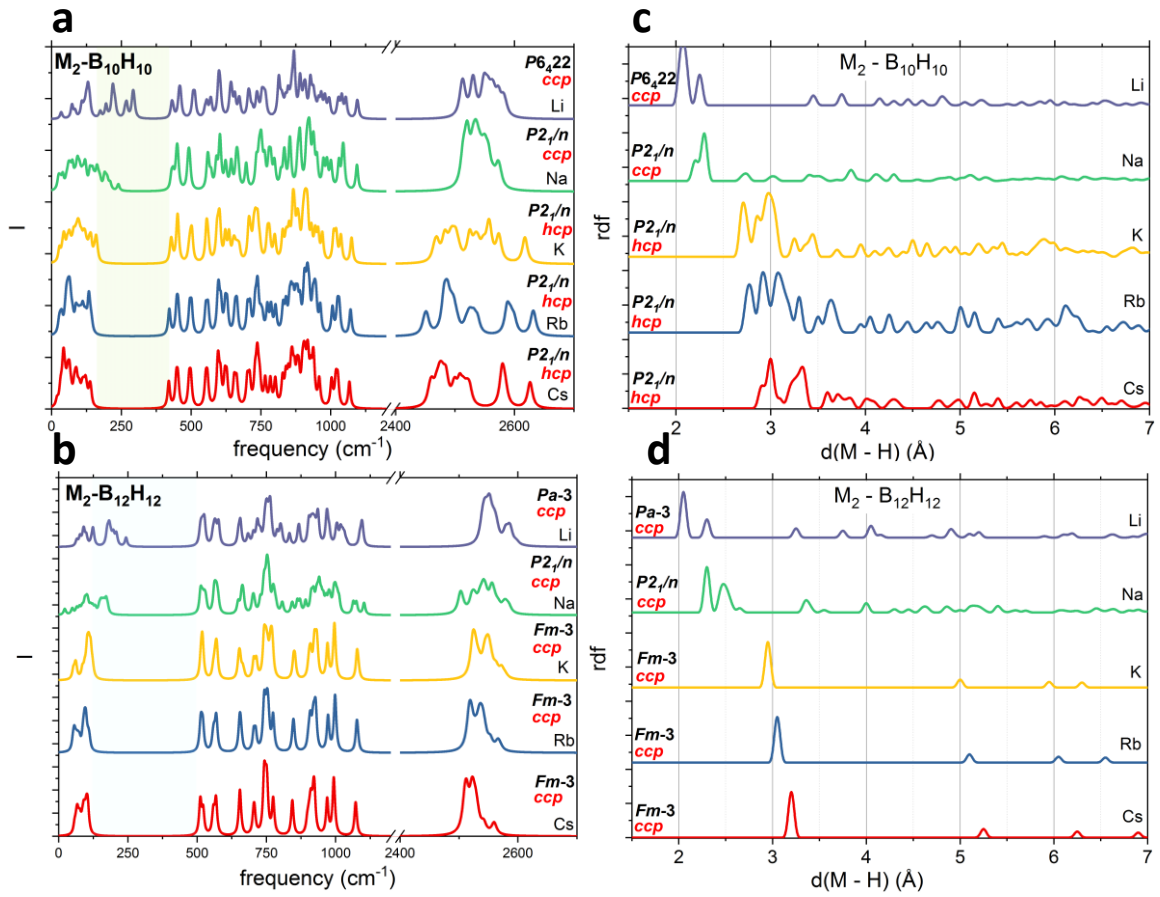

Figure 6. Distribution of the phonon distribution at the Γ-point for alkali metal deca H-*c*-B (a) and dodeca H-*c*-B (b), and the radial distribution function for cation – hydrogen separation for alkali metal deca H-*c*-B (c) and dodeca H-*c*-B (d). The calculated frequencies are broaden with 5 cm^{-1} Lorentzian.

The short metal – hydrogen distances for two lightest metals are correlated with broader range of their lattice modes and indicate direct M – H interaction. This is most apparent for $Li_2B_{10}H_{10}$. From the Pauling rules for ionic compounds the coordination of metals can be estimated from the ratio of ionic radii of anion and cations.[39] This is particularly well observed in metal hydridoborates, where one can assume radii of $B_{10}H_{10}^{2-}$ as 6.0 Å (5.8 Å for $B_{12}H_{12}^{2-}$). Size of alkali metal cations increases with atomic number and according to Shannon radii is:[40] 1.2 Å for Li, 1.9 Å for Na, 2.66 Å for K, 2.96 Å for Rb, and 3.38 Å for Cs. The ionic size ratio for compounds with $B_{10}H_{10}^{2-}$ anions is: 0.20 for Li (3), 0.32 for Na (4), 0.44 for K (6), 0.49 for Rb (6), and 0.56 for Cs (6); numbers in parentheses indicate coordination number for anion. For compounds with $B_{12}H_{12}^{2-}$ anions formal coordination numbers are the same. In fact for all these compounds cations are located within coordination tetrahedra between nearest anions, as even for heavier alkali metals the ratio is close to 0.414 that is the limit of

tetrahedral coordination. The structure analysis indicates that in $P2_1/c$ structure of $(K,Rb,Cs)_2B_{10}H_{10}$ half of cations are located at octahedral voids. Exceptions are Li and Na, where each cation is surrounded by three anions, thus is located at the face of coordination tetrahedra. Relation between coordination number and lattice type is known to correlate with ionic conductivity,[31,41] and *bcc* anion packing is ultimate for the best ion conductor.

In **Fig. 7** we present coordination polyhedra for $B_{10}H_{10}$ anions by Li and Na. Such presentation reveals highly symmetric polyhedra for Li and Na. The positions of cations follow *D*4*d* symmetry of the anion, forming a deformed cubic coordination for $Na_2B_{10}H_{10}$, and six Li cations surround the anion in $Li_2B_{10}H_{10}$. Among the symmetry elements of *D*4*d* point group of capped square antiprism that is $B_{10}H_{10}$ only these related to rotations are accessible due to thermal excitations, see **Fig. 7**. Improper rotation by 45° (S_8) without reflection is the less energy demanding process that preserves orientation of anions in the crystal opening additional sites for cations. This process will not change the hexagonal symmetry of the low temperature phase. Rotation around one of C_2 axes by 90° changes anion orientation in the crystal lattice thus breaks *a*,*b*,*a*,*b* stacking of *hcp* lattice. This is in fact observed in the high temperature *ccp* structure of this compound, where the anions are still aligned along principal lattice directions with cations distributed in the tetrahedral void with similar Li – H separations as in the LT phase. The strong Li – H interaction in $Li_2B_{10}H_{10}$ is also related to low thermal expansion of this compound within the H-*c*-B class (see **Table 2**). As shown in **Fig. 6 c** for any configuration considered in the cubic phase the shortest distance between hydrogen and lithium do not increase above 2.1 Å which is equivalent to the fact that with increasing separation between anions the compound disintegrate into molecular entities consisting of cations and anions.

In the phase transition of $Na_2B_{10}H_{10}$ from the low temperature $P2_1/c$ structure to the cubic *Fm*-3*m* one is related to orientational disorder of anions, while eight Na^+ effectively forms regular cubic coordination around an anion (**Fig. 7**). This is related with disorder in the cationic sublattice but not with changes of the anion coordination number.

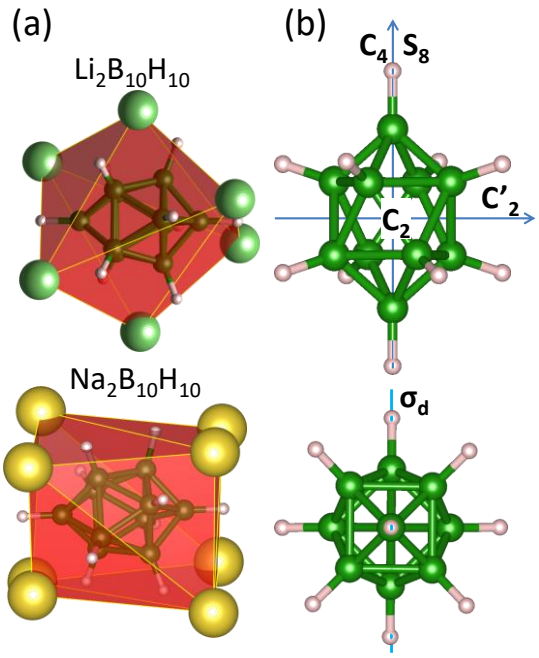

Figure 7. Coordination polyhedra for $B_{10}H_{10}^{2-}$ anions in alkali metal deca H-*c*-B. Small green/gray spheres are for boron/hydrogen; large green are Li, yellow – Na (a). The schematic view of the symmetry elements of D4d point group of $B_{10}H_{10}^{2-}$ anion: C_4/ S_8 are rotations/improper rotations around four-fold and eight-fold axis, C_2/C'_2 are rotations around two-fold axis, and σ_d stands for the mirror plane (b).

Conclusion

In this work a class of compounds, namely hydrido-*closo*-borates, has been subject to structural investigation using *in situ* XRD methods under external pressure and temperature stimuli, combined with DFT calculations. Those materials have demonstrated very high compressibility and very low shear moduli revealing highly malleable materials which would allow fast structural reconstruction under mechanical stresses. Furthermore, this family of compounds has exhibited very high CTE, two orders of magnitude higher than oxides. Interestingly, our investigations discover two new crystal phases, the first one for $K_2B_{12}H_{12}$ resulting from the pressure induced phase transition around 2 GPa toward *Pnnm* symmetry and the second phase for which the transition is induced by the temperature and transforms $Li_2B_{10}H_{10}$ from $P6_422$ to *Pa*-3 symmetry as suggested by DFT calculations. The present study allows completing knowledge about the crystal chemistry of this astonishing class of compounds and further confirms their trend for the *ccp* underlying anions packing.

Experimental.

PXRD

Samples were purchased from Katchem company. The sample was measured at the Swiss-Norwegian Beam Lines BM01 of the European Synchrotron Radiation Facility in Grenoble, France. A 2D image plate detector Pilatus 2M positioned at 411 mm from the sample was used with a wavelength of 0.71414 Å. The 2D diffraction patterns were integrated with Bubble software.[42] The sample detector geometry was calibrated with a LaB_6 NIST standard. For high pressure experiments the Diamond Anvil Cell (DAC), with flat culet of diameter 600 µm, was

loaded in an argon filled glove box (MBraun O_2<0.1 ppm, H_2O<0.1ppm). The samples were loaded with ruby crystals, for pressure calibration, into a hole of 250 μm drilled in a stainless-steel gasket. No pressure transmitting media was used owing to the low bulk modulus of these families of materials. For high temperature experiments, the samples were loaded in 0.5 mm glass capillary in the glove box. The temperature was controlled using a Cyberstar hot blower. For hp-β-$K_2B_{12}H_{12}$ and ht-β-$Li_2B_{10}H_{10}$ the structure were solved using the isostructural models hp3-ζ-$Na_2B_{12}H_{12}$ and rt-α-$Li_2B_{12}H_{12}$ manual adjustment of the cell parameters were done prior to their refinement using Pawley algorithm implemented in TOPAS,[43] this algorithm was used also for the refinement of the cell parameters as a function of temperature and pressure. The refinements of the structure were performed using the Rietveld method,[44] in the TOPAS program.[43] For the hp polymorph spherical harmonic approach was used to simulate the strong preferential orientation caused by the DAC. The cell parameters as a function of temperature and pressure were refined using Pawley algorithm.

DFT calculations

Calculations were performed within density functional theory (DFT) with periodic plane wave basis set as implements in Vienna ab initio Simulation Package.[45,46] The calculations parameters were: cutoff energy for the basis set expansion 700 eV; the k-point sampling density k·a ≥ 20; the convergence criteria for the electronic degrees of freedom was 10^{-6} eV/A; for the structural relaxations the conjugated gradient method with convergence 10^{-2} eV/A was used; Projected Augmented Wave Potentials (PAW)[47,48] were used for atoms with the electronic configuration ($1s^1$) for H, ($2s^22p^1$) for B, ($1s^22s^1$) for Li, ($2p^63s^1$) for Na , ($3p^64s^1$) for K , ($4p^65s^1$) for Rb , ($5p^66s^1$) for Cs. The gradient corrected (GGA) exchange – correlation functional and the non-local corrections accounting for a weak dispersive interactions were applied.[49–51] The normal modes at the Γ-point were calculated in the real space with atomic displacements ±0.1 Å in all symmetry inequivalent directions, and visualized by placing Lorentzians with half-width 5 cm^{-1} for each mode. The normal mode frequencies were obtained by direct diagonalization of the dynamical matrix obtained from the forces calculated for displaced configurations. Elastic constants were calculated via deformation of the unit cell, ±1% in each relevant direction and angle. For normal mode and elastic properties fully optimized structures were used.

Acknowledgements.

We thank V. Dmitriev, I. Dovgaliuk and D. Chernyshov of the SNBL at ESRF for their support with the high-pressure experiments. We thank the financial support from the SNSF Sinergia project CRSII2_160749 and the SNSF project 200021_169033/1. Z.L. acknowledges NCN support through 2019/01/Y/ST5/00046 project and CPU allocation at PL-Grid infrastructure.

Associated content.

Supporting Information available: Calculation procedure for ht-$Li_2B_{10}H_{10}$, the result of the Rietveld refinement, of the free energy as a function of the pressure and the transformation of the structures from *Pnnm* to $P2_1/c$ for hp-$K_2B_{12}H_{12}$ (Fig. S1-4). The evolution of the cell volume as a function of the pressure (Fig. S5) and the orientation of $B_{10}H_{10}^{2-}$ anions of for ht-$Li_2B_{10}H_{10}$ with *Fm*-3*m* and *Pa*-3 space group (Fig S6).

ORCID

Romain Moury: 0000-0002-1198-2586
Zbigniew Lodziana: 0000-0002-4713-6891
Arndt Remhof: 0000-0002-8394-9646
Léo Duchêne: 0000-0003-0309-4682
Elsa Roedern: 0000-0002-8002-6723
Angelina Gigante: 0000-0002-7226-1360
Hans Hagemann: 0000-0002-7183-8543

References.

(1) Udovic, T. J.; Matsuo, M.; Unemoto, A.; Verdal, N.; Stavila, V.; Skripov, A. V.; Rush, J. J.; Takamura, H.; Orimo, S. I. "Sodium Superionic Conduction in $Na_2B_{12}H_{12}$". *Chem. Commun.* **2014**, *50* (28), 3750–3752. https://doi.org/10.1039/C3CC49805K.

(2) Hansen, B. R. S. S.; Paskevicius, M.; Li, H.-W. W.; Akiba, E.; Jensen, T. R. "Metal Boranes: Progress and Applications". *Coord. Chem. Rev.* **2016**, *323*, 60–70. https://doi.org/10.1016/j.ccr.2015.12.003.

(3) Duchêne, L.; Remhof, A.; Hagemann, H.; Battaglia, C. "Status and Prospects of Hydroborate Electrolytes for All-Solid-State Batteries". *Energy Storage Mater.* **2020**, *25*, 782–794. https://doi.org/10.1016/J.ENSM.2019.08.032.

(4) Brighi, M.; Murgia, F.; Černý, R. "Closo-Hydroborate Sodium Salts as an Emerging Class of Room-Temperature Solid Electrolytes". *Cell Reports Phys. Sci.* **2020**, *1* (10), 100217. https://doi.org/10.1016/J.XCRP.2020.100217.

(5) Kim, S.; Oguchi, H.; Toyama, N.; Sato, T.; Takagi, S.; Otomo, T.; Arunkumar, D.; Kuwata, N.; Kawamura, J.; Orimo, S. ichi. "A Complex Hydride Lithium Superionic Conductor for High-Energy-Density All-Solid-State Lithium Metal Batteries". *Nat. Commun.* **2019**, *10* (1), 1–9. https://doi.org/10.1038/s41467-019-09061-9.

(6) Brighi, M.; Murgia, F.; Łodziana, Z.; Schouwink, P.; Wołczyk, A.; Černý, R. "A Mixed Anion Hydroborate/Carba-Hydroborate as a Room Temperature Na-Ion Solid Electrolyte". *J. Power Sources* **2018**, *404*, 7–12. https://doi.org/10.1016/J.JPOWSOUR.2018.09.085.

(7) Tang, W. S.; Yoshida, K.; Soloninin, A. V; Skoryunov, R. V; Babanova, O. A.; Skripov, A. V; Dimitrievska, M.; Stavila, V.; Orimo, S.; Udovic, T. J. "Stabilizing Superionic-Conducting Structures via Mixed-Anion Solid Solutions of Monocarba- Closo -Borate Salts". *ACS Energy Lett.* **2016**, *1* (4), 659–664. https://doi.org/10.1021/acsenergylett.6b00310.

(8) Tang, W. S.; Matsuo, M.; Wu, H.; Stavila, V.; Zhou, W.; Talin, A. A.; Soloninin, A. V; Skoryunov, R. V; Babanova, O. A.; Skripov, A. V; Unemoto, A.; Orimo, S.-I.; Udovic, T. J.; Tang, W. S.; Wu, H.; Zhou, W.; Udovic, T. J.; Matsuo, M.; Orimo, S.; Stavila, V.; Talin, A. A.; Nanomaterials, E.; Soloninin, A. V; Skoryunov, R. V; Babanova, O. A.; Skripov, A. V; Unemoto, A. "Liquid-Like Ionic Conduction in Solid Lithium and Sodium Monocarba-Closo-Decaborates Near or at Room Temperature". *Adv. Energy Mater.* **2016**, *6* (8), 1502237. https://doi.org/10.1002/AENM.201502237.

(9) Payandeh, S. H.; Rentsch, D.; Łodziana, Z.; Asakura, R.; Bigler, L.; Černý, R.; Battaglia, C.; Remhof, A. "Nido-Hydroborate-Based Electrolytes for All-Solid-State Lithium Batteries". *Adv. Funct. Mater.* **2021**, *31* (18), 2010046. https://doi.org/10.1002/ADFM.202010046.

(10) Payandeh, S.; Asakura, R.; Avramidou, P.; Rentsch, D.; Łodziana, Z.; Černý, R.; Remhof, A.; Battaglia, C. "Nido-Borate/ Closo-Borate Mixed-Anion Electrolytes for All-Solid-State Batteries". *Chem. Mater.* **2020**, *32* (3), 1101–1110. https://doi.org/10.1021/ACS.CHEMMATER.9B03933/SUPPL_FILE/CM9B03933_SI_006.CIF.

(11) Fisher, S. P.; Tomich, A. W.; Lovera, S. O.; Kleinsasser, J. F.; Guo, J.; Asay, M. J.; Nelson, H. M.; Lavallo, V. "Nonclassical Applications of Closo-Carborane Anions: From Main Group Chemistry and Catalysis to Energy Storage". *Chem. Rev.* **2019**, *119* (14), 8262–8290. https://doi.org/10.1021/ACS.CHEMREV.8B00551.

(12) Jørgensen, M.; Shea, P. T.; Tomich, A. W.; Varley, J. B.; Bercx, M.; Lovera, S.; Černý, R.; Zhou, W.; Udovic, T. J.; Lavallo, V.; Jensen, T. R.; Wood, B. C.; Stavila, V. "Understanding Superionic Conductivity in Lithium and Sodium Salts of Weakly Coordinating Closo-Hexahalocarbaborate Anions". *Chem. Mater.* **2020**, *32* (4), 1475–1487. https://doi.org/10.1021/ACS.CHEMMATER.9B04383/SUPPL_FILE/CM9B04383_SI_004.CIF.

(13) Muetterties, E. L.; Balthis, J. H.; Chia, Y. T.; Knoth, W. H.; Miller, H. C.; L. Muetterties, E.; H. Balthis, J.; T. Chia, Y.; H. Knoth, W.; C. Miller, H. "Chemistry of Boranes. VIII. Salts and Acids of $B_{10}H_{10}^{-2}$ and $B_{12}H_{12}^{-2}$". *Inorg. Chem.* **2002**, *3* (3), 444–451.

(14) Asakura, R.; Duchêne, L.; Kühnel, R. S.; Remhof, A.; Hagemann, H.; Battaglia, C. "Electrochemical Oxidative Stability of Hydroborate-Based Solid-State Electrolytes". *ACS Appl. Energy Mater.* **2019**, *2* (9), 6924–6930. https://doi.org/10.1021/ACSAEM.9B01487/SUPPL_FILE/AE9B01487_SI_001.PDF.

(15) Duchêne, L.; Kühnel, R.-S.; Stilp, E.; Cuervo Reyes, E.; Remhof, A.; Hagemann, H.; Battaglia, C. "A Stable 3 V All-Solid-State Sodium–Ion Battery Based on a Closo -Borate Electrolyte". *Energy Environ. Sci.* **2017**, *10* (12), 2609–2615. https://doi.org/10.1039/C7EE02420G.

(16) Murgia, F.; Brighi, M.; Černý, R. "Room-Temperature-Operating Na Solid-State Battery with Complex Hydride as Electrolyte". *Electrochem. commun.* **2019**, *106*, 106534. https://doi.org/10.1016/J.ELECOM.2019.106534.

(17) Moury, R.; Gigante, A.; Hagemann, H. "An Alternative Approach to the Synthesis of NaB_3H_8 and $Na_2B_{12}H_{12}$ for Solid Electrolyte Applications". *Int. J. Hydrogen Energy* **2016**, 10–14. https://doi.org/10.1016/j.ijhydene.2017.02.044.

(18) Gigante, A.; Duchêne, L.; Moury, R.; Pupier, M.; Remhof, A.; Hagemann, H. "Direct Solution-Based Synthesis of $Na_4(B_{12}H_{12})(B_{10}H_{10})$ Solid Electrolyte". *ChemSusChem* **2019**, *12* (21). https://doi.org/10.1002/cssc.201902152.

(19) Duchêne, L.; Kim, D. H.; Song, Y. B.; Jun, S.; Moury, R.; Remhof, A.; Hagemann, H.; Jung, Y. S.; Battaglia, C. "Crystallization of Closo-Borate Electrolytes from Solution Enabling Infiltration into Slurry-Casted Porous Electrodes for All-Solid-State Batteries". *Energy Storage Mater.* **2020**, *26*. https://doi.org/10.1016/j.ensm.2019.11.027.

(20) Brighi, M.; Murgia, F.; Černý, R.; Brighi, M.; Murgia, F.; Černý, R. "Mechanical Behavior and Dendrite Resistance of Closo-Hydroborate Solid Electrolyte". *Adv. Mater. Interfaces* **2021**, 2101254. https://doi.org/10.1002/ADMI.202101254.

(21) Asakura, R.; Reber, D.; Duchêne, L.; Payandeh, S.; Remhof, A.; Hagemann, H.; Battaglia, C. "4 V Room-Temperature All-Solid-State Sodium Battery Enabled by a Passivating Cathode/Hydroborate Solid Electrolyte Interface". *Energy Environ. Sci.* **2020**, *13* (12), 5048–5058. https://doi.org/10.1039/D0EE01569E.

(22) Frenck, L.; Sethi, G. K.; Maslyn, J. A.; Balsara, N. P. "Factors That Control the Formation of Dendrites and Other Morphologies on Lithium Metal Anodes". *Front. Energy Res.* **2019**, *7*, 115. https://doi.org/10.3389/FENRG.2019.00115/BIBTEX.

(23) Sau, K.; Ikeshoji, T.; Takagi, S.; Orimo, S. ichi; Errandonea, D.; Chu, D.; Cazorla, C. "Colossal Barocaloric Effects in the Complex Hydride Li2B12H12". *Sci. Rep.* **2021**, *11* (1), 1–9. https://doi.org/10.1038/s41598-021-91123-4.

(24) Černý, R.; Brighi, M.; Murgia, F. "The Crystal Chemistry of Inorganic Hydroborates". *Chem.*

2020, Vol. 2, Pages 805-826 **2020**, *2* (4), 805–826. https://doi.org/10.3390/CHEMISTRY2040053.

(25) Wu, H.; Tang, W. S.; Stavila, V.; Zhou, W.; Rush, J. J.; Udovic, T. J. "Structural Behavior of Li2B10H10". *J. Phys. Chem. C* **2015**, *119* (12), 6481–6487. https://doi.org/10.1021/ACS.JPCC.5B00533.

(26) Verdal, N.; Wu, H.; Udovic, T. J.; Stavila, V.; Zhou, W.; Rush, J. J. "Evidence of a Transition to Reorientational Disorder in the Cubic Alkali-Metal Dodecahydro-Closo-Dodecaborates". *J. Solid State Chem.* **2011**, *184* (11), 3110–3116. https://doi.org/10.1016/J.JSSC.2011.09.010.

(27) Moury, R.; Łodziana, Z.; Remhof, A.; Duchêne, L.; Roedern, E.; Gigante, A.; Hagemann, H.; IUCr. "Pressure-Induced Phase Transitions in $Na_2B_{12}H_{12}$, Structural Investigation on a Candidate for Solid- State Electrolyte". *Acta Crystallogr. Sect. B Struct. Sci. Cryst. Eng. Mater.* **2019**, *75* (3), 406–413. https://doi.org/10.1107/S2052520619004670.

(28) Benham, V.; Lord, G.; Butler, I. S.; Gilson, D. F. R. "High-Pressure Diamond-Anvil-Cell Micro-Raman Spectra of Mercuric Cyanide, $Hg(CN)_2$, and Cesium Dodecahydroborate, $Cs_2[B_{12}H_{12}]$:". *Appl. Spectorscopy* **1987**, *41* (5), 915–917. https://doi.org/10.1366/0003702874448030.

(29) Paskevicius, M.; Pitt, M. P.; Brown, D. H.; Sheppard, D. A.; Chumphongphan, S.; Buckley, C. E. "First-Order Phase Transition in the $Li_2B_{12}H_{12}$ System". *Phys. Chem. Chem. Phys.* **2013**, *15* (38), 15825–15828. https://doi.org/10.1039/C3CP53090F.

(30) Verdal, N.; Her, J. H.; Stavila, V.; Soloninin, A. V.; Babanova, O. A.; Skripov, A. V.; Udovic, T. J.; Rush, J. J. "Complex High-Temperature Phase Transitions in $Li_2B_{12}H_{12}$ and $Na_2B_{12}H_{12}$". *J. Solid State Chem.* **2014**, *212*, 81–91. https://doi.org/10.1016/J.JSSC.2014.01.006.

(31) Wang, Y.; Richards, W. D.; Ong, S. P.; Miara, L. J.; Kim, J. C.; Mo, Y.; Ceder, G. "Design Principles for Solid-State Lithium Superionic Conductors". *Nat. Mater.* **2015**, *14* (10), 1026–1031. https://doi.org/10.1038/nmat4369.

(32) Schranz, W.; Tröster, A.; Koppensteiner, J.; Miletich, R. "Finite Strain Landau Theory of High Pressure Phase Transformations". *J. Phys. Condens. Matter* **2007**, *19* (27), 275202. https://doi.org/10.1088/0953-8984/19/27/275202.

(33) Orobengoa, D.; Capillas, C.; Aroyo, M. I.; Perez-Mato, J. M. "AMPLIMODES: Symmetry-Mode Analysis on the Bilbao Crystallographic Server". *J. Appl. Crystallogr.* **2009**, *42* (5), 820–833. https://doi.org/10.1107/S0021889809028064.

(34) Perez-Mato, J. M.; Orobengoa, D.; Aroyo, M. I. "Mode Crystallography of Distorted Structures". *Acta Crystallogr. Sect. A Found. Crystallogr.* **2010**, *66* (5), 558–590. https://doi.org/10.1107/S010876731001624 7/SH5107SUP1.PDF.

(35) Wang, Z. Q.; Wu, M. S.; Liu, G.; Lei, X. L.; Xu, B.; Ouyang, C. Y. "Elastic Properties of New Solid State Electrolyte Material $Li_{10}GeP_2S_{12}$: A Study from First-Principles Calculations". *Int. J. Electrochem. Sci* **2014**, *9*, 562–568.

(36) Pugh, S. F. "XCII. Relations between the Elastic Moduli and the Plastic Properties of Polycrystalline Pure Metals". *London, Edinburgh, Dublin Philos. Mag. J. Sci.* **2009**, *45* (367), 823–843. https://doi.org/10.1080/14786440808520496.

(37) Sethio, D.; Lawson Daku, L. M.; Hagemann, H. "A Theoretical Study of the Spectroscopic Properties of B_2H_6 and of a Series of $B_xH_y^{z-}$ Species (x = 1−12, y = 3−14, z = 0−2): From BH_3 to $B_{12}H_{12}^{2-}$". *Int. J. Hydrogen Energy* **2016**, *41* (16), 6814–6824. https://doi.org/10.1016/J.IJHYDENE.2016.02.121.

(38) Hagemann, H.; Sharma, M.; Sethio, D.; Lawson Daku, L. M. "Correlating Boron–Hydrogen Stretching Frequencies with Boron–Hydrogen Bond Lengths in Closoboranes: An Approach

Using DFT Calculations". *Helv. Chim. Acta* **2018**, *101* (2), e1700239. https://doi.org/10.1002/HLCA.201700239.

(39) Pauling, L. "The Principles Determining the Structure of Complex Ionic Crystals". *J. Am. Chem. Soc.* **1929**, *51* (4), 1010–1026. https://doi.org/10.1021/JA01379A006.

(40) Shannon, R. D.; IUCr. "Revised Effective Ionic Radii and Systematic Studies of Interatomic Distances in Halides and Chalcogenides". *Acta Crystallogr. Sect. A* **1976**, *32* (5), 751–767. https://doi.org/10.1107/S0567739476001551.

(41) Sadikin, Y.; Schouwink, P.; Brighi, M.; Łodziana, Z.; Černý, R. "Modified Anion Packing of $Na_2B_{12}H_{12}$ in Close to Room Temperature Superionic Conductors". *Inorg. Chem.* **2017**, *56* (9), 5006–5016. https://doi.org/10.1021/ACS.INORGCHEM.7B00013/SUPPL_FILE/IC7B00013_SI_002.ZIP.

(42) Dyadkin, V.; Pattison, P.; Dmitriev, V.; Chernyshov, D. "A New Multipurpose Diffractometer PILATUS@SNBL". *J. Synchrotron Radiat.* **2016**, *23* (3), 825–829. https://doi.org/10.1107/S1600577516002411.

(43) Coelho, A. A. "Whole-Profile Structure Solution from Powder Diffraction Data Using Simulated Annealing". *J. Appl. Crystallogr.* **2000**, *33* (3), 899–908. https://doi.org/10.1107/S002188980000248X.

(44) Rietveld, H. M. "A Profile Refinement Method for Nuclear and Magnetic Structures". *J. Appl. Crystallogr.* **1969**, *2* (2), 65–71. https://doi.org/10.1107/S0021889869006558.

(45) Kresse, G.; Furthmüller, J. "Efficient Iterative Schemes for *Ab Initio* Total-Energy Calculations Using a Plane-Wave Basis Set". *Phys. Rev. B* **1996**, *54* (16), 11169. https://doi.org/10.1103/PhysRevB.54.11169.

(46) Kresse, G.; Furthmüller, J. "Efficiency of Ab-Initio Total Energy Calculations for Metals and Semiconductors Using a Plane-Wave Basis Set". *Comput. Mater. Sci.* **1996**, *6* (1), 15–50. https://doi.org/10.1016/0927-0256(96)00008-0.

(47) Blöchl, P. E. "Projector Augmented-Wave Method". *Phys. Rev. B* **1994**, *50* (24), 17953. https://doi.org/10.1103/PhysRevB.50.17953.

(48) Kresse, G.; Joubert, D. "From Ultrasoft Pseudopotentials to the Projector Augmented-Wave Method". *Phys. Rev. B* **1999**, *59* (3), 1758. https://doi.org/10.1103/PhysRevB.59.1758.

(49) Perdew, J. P.; Burke, K.; Ernzerhof, M. "Generalized Gradient Approximation Made Simple". *Phys. Rev. Lett.* **1996**, *77* (18), 3865. https://doi.org/10.1103/PhysRevLett.77.3865.

(50) Dion, M.; Rydberg, H.; Schröder, E.; Langreth, D. C.; Lundqvist, B. I. "Van Der Waals Density Functional for General Geometries". *Phys. Rev. Lett.* **2004**, *92* (24), 246401. https://doi.org/10.1103/PHYSREVLETT.92.246401/FIGURES/4/MEDIUM.

(51) Maniadaki, A. E.; Łodziana, Z. "Theoretical Description of Alkali Metal Closo-Boranes – towards the Crystal Structure of $MgB_{12}H_{12}$". *Phys. Chem. Chem. Phys.* **2018**, *20* (48), 30140–30149. https://doi.org/10.1039/C8CP02371A.

Table of Content

Synopsis. Herein we studied the pressure and temperature dependancies of alkali hydrido-*closo*-borates to extract mechanical propertie of this class of compound which have promising future as solid electrolyte. In our search, we have discovered and have solved two new high pressure and high temperature crystal structures.